Biochimica et Biophysica Acta 1838 (2014) 3107–3117

Contents lists available at ScienceDirect

Biochimica et Biophysica Acta

journal homepage: www.elsevier.com/locate/bbamem

# Conformational heterogeneity of α-synuclein in membrane

Josh V. Vermaas, Emad Tajkhorshid *

*Beckman Institute for Advanced Science and Technology, Department of Biochemistry, College of Medicine, and Center for Biophysics and Computational Biology, University of Illinois at Urbana-Champaign, Urbana, IL 61801, USA*

ARTICLE INFO

*Article history:*
Received 26 March 2014
Received in revised form 9 August 2014
Accepted 11 August 2014
Available online 16 August 2014

*Keywords:*
Membrane binding
α-Synuclein
Peripheral membrane protein
Molecular dynamics
HMMM

ABSTRACT

α-Synuclein (αS) is a natively disordered protein in solution, thought to be involved in the fusion of neurotransmitter vesicles to cellular membranes during neurotransmission. Monomeric αS has been previously characterized in two distinct membrane-associated conformations: a broken-helix structure, and an extended helix. By employing atomistic molecular dynamics and a novel membrane representation with significantly enhanced lipid mobility (HMMM), we investigate the process of spontaneous membrane binding of αS and the conformational dynamics of monomeric αS in its membrane-bound form.

By repeatedly placing helical αS monomers in solution above a planar lipid bilayer and observing their spontaneous association and its spontaneous insertion into the membrane during twenty independent unbiased simulations, we are able to characterize αS in its membrane-bound state, suggesting that αS has a highly variable membrane insertion depth at equilibrium. Our simulations also capture two distinct states of αS, the starting broken-helix conformation seen in the micelle bound NMR structures, and a semi-extended helix. Analysis of lipid distributions near αS monomers indicates that the transition to a semi-extended helix is facilitated by concentration of phosphatidyl-serine headgroups along the inner edge of the protein. Such a lipid-mediated transition between helix–turn–helix and extended conformations of αS may also occur in vivo, and may be important for the physiological function of αS.



## 1. Introduction

α-Synuclein (αS) is a 14 kDa protein that is thought to play a role in synaptic vesicle fusion [1,2]. The protein is, however, mostly known for its involvement in human pathological conditions such as Parkinson's disease, in which αS aggregates form Lewy bodies, the pathological characteristic of such diseases [3,4]. These aggregates are known to form as a result of three distinct point mutations [5–7], or from overexpression of αS [8,9]. A clear physiological role for αS within cells has not been uniquely identified [10]; however, αS has been shown to localize to nerve termini [11–13], bind copper [14], and play a role in the uptake and release of neurotransmitters from vesicles [1,2,15–18], as well as in the regulation of glucose uptake [19]. αS has also been shown to interact with proteins involved in lipid metabolism [20,21], and binds to negatively charged lipids [22]. The formation of Lewy bodies through αS fibrilation and aggregation is a process that is not fully understood, but evidence suggests a close link to αS interaction with anionic phospholipids [23–25] or to acidic conditions [26]. It has been suggested that intermediate oligomeric states of αS disrupt membranes, and are particularly toxic to neurons [27–30].

Since a large part of αS physiology is membrane-dependent, recent studies have focused on its interaction with biological membranes [28,31], with the primary goal of characterizing the membrane-bound conformation of αS in vitro. Some have suggested that only αS aggregates bind to membranes [26], or that αS binds as a tetramer [32]. In contrast, the available NMR/EPR structures of αS on micelles are indicative of a monomeric horseshoe-like broken-helix conformation [33–35]. ESR and DEER measurements, on the other hand, suggest that αS monomers adopt an extended helical structure in the membrane [36–39]. There is considerable evidence that the geometry of the membrane plays a crucial role in determining the conformation of αS [40,41], but there is also evidence of interconversion between membrane-bound extended and broken-helix conformations [42,43], favoring the extended helix by a ratio of 7.6:1 [44]. Long term NMR experiments also show that the initial membrane-bound helical structures undergo further transitions to fibril-like structures over the course of several days [45]. The transition between unfolded states in solution and a primarily helical membrane-bound state for αS is thought to be driven by the first 15–25 N-terminal residues [46–51].

In addition to this wealth of experimental information, computational studies have supplemented our understanding of αS dynamics. Molecular dynamics (MD) is an excellent tool for probing spatial and temporal resolutions that are difficult for typical experiments to achieve. Prior MD studies have given us additional insight into the role that membranes play in αS function. An atomistic MD study investigated the membrane-bound form of a broken-helix structure by initially placing it within the membrane, suggesting that neighboring glycine

* Corresponding author. Tel.: +1 217 244 6914.
*E-mail address:* emad@life.illinois.edu (E. Tajkhorshid).

http://dx.doi.org/10.1016/j.bbamem.2014.08.012
0005-2736/

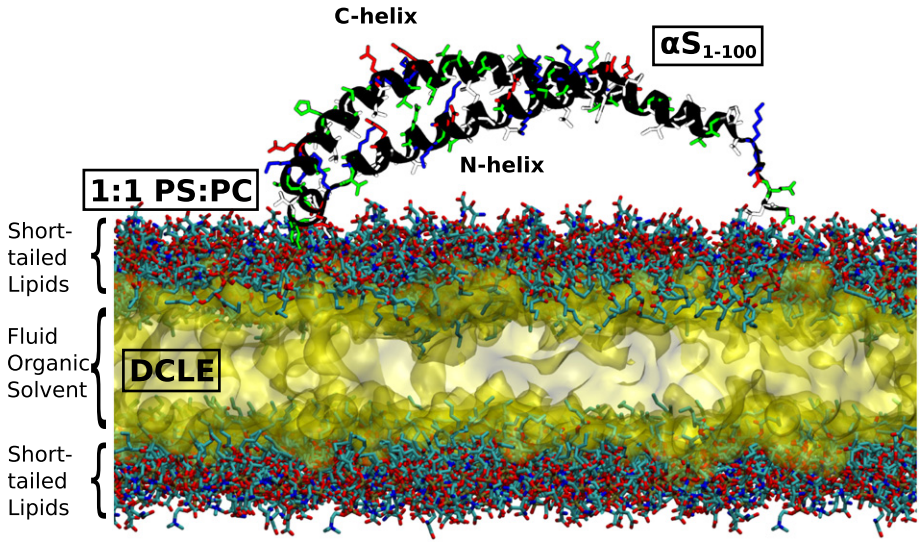


**Fig. 1.** Initial simulation system setup. The protein structure (shown as a black cartoon and sidechains colored according to their polarity, blue are positively charged, red are negatively charged, green are positively charged and white are nonpolar) is placed above the HMMM headgroups, shown here with each heavy atom represented as a colored element (carbon is cyan, oxygen is red, phosphorus is brown and nitrogen is red) and packed in with explicit DCLE solvent, shown as a yellow surface.

residues are the flexible segments of membrane-bound αS [52]. Other studies have focused on the pore-formation of αS aggregates [28,53], membrane binding of the N-terminus [48], or the membrane curvature induced by binding of αS [54].

What is missing from this picture is an unbiased description of the membrane associated states of αS, especially as it relates to the role of specific lipid–protein interactions in shaping the membrane-bound conformation. Earlier atomistic simulations of the conformational dynamics of αS initially placed αS within the bilayer, and removed lipids to accommodate the added bulk [52]. In this context, the slow dynamics of lipid molecules, $D \sim 8 \times 10^{-8}$ cm$^2$ s$^{-1}$ [55,56], poses a problem, as the slow lipid dynamics restrict membrane reorganization around the protein. The slow lipid dynamics are only compounded by the addition of αS, and increase the relaxation time of the membrane by two orders of magnitude [54]. For typical atomistic MD simulation times on the order of hundreds of nanoseconds, lipids simply do not move and interchange frequently enough to sample the space efficiently, and result in inadequate sampling for more than a qualitative description of individual protein–lipid interactions.

This problem is well recognized, and may be addressed through various methodologies. Some choose to simplify the model through the use of coarse graining, which permits longer timescales at the cost

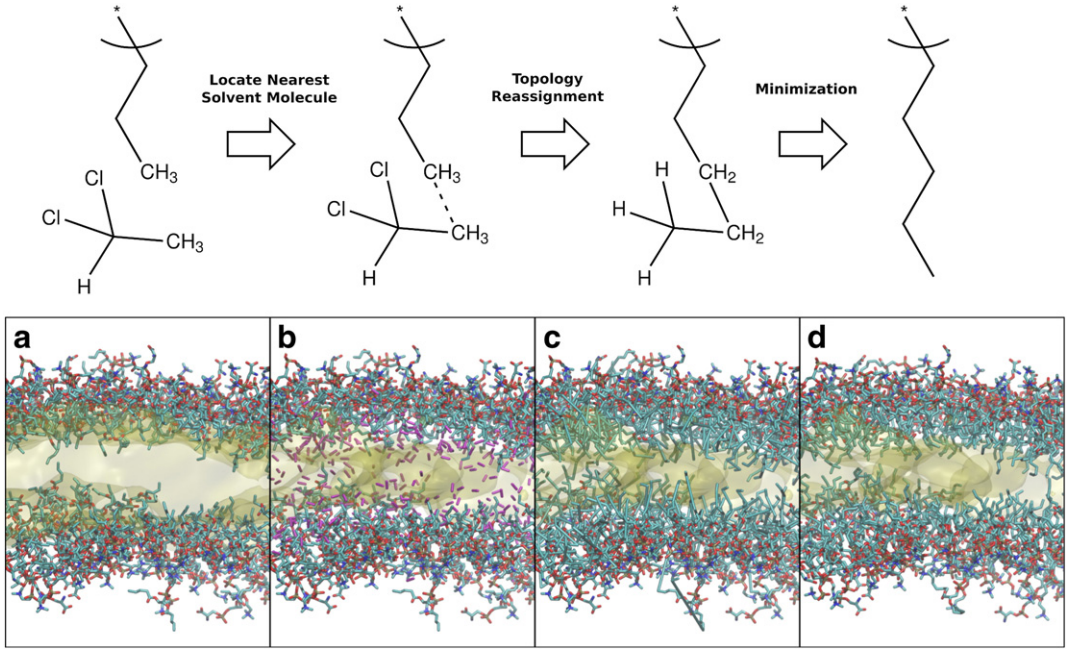


**Fig. 2.** Schematic of the lipid extension process (top) and an example round of tail extension (bottom). In the first step, the terminal methyl group of a short lipid finds the closest carbon in a solvent DCLE molecule. In the second step, the underlying structures are patched, first by adding the bond between the carbons, and then deleting and retyping the appropriate atoms to add two carbons to the chain. The resulting structure is then minimized before simulation to eliminate the long bonds that result from the joining of two initially disjoint molecules. The resulting lipid tail is thus 2 carbons longer than the original lipid. Given in (a) is the initial membrane structure, as taken from the end of the HMMM equilibration simulation. The lipid heavy atoms are shown explicitly with the following color scheme: carbons are cyan, nitrogens are blue, oxygens are red, and phosphorus atoms are brown. The organic solvent is shown as a transparent yellow surface representation [74]. In (b), the nearest unique solvent carbons are highlighted in purple, and (c) shows the initial bonded structure. (d) shows the resulting structure after the minimization.

of atomic detail [54,57]. Monte Carlo approaches have been used to treat binary lipid systems [58], however such approaches by their nature are of limited utility when investigating the details of a transition. We will be using a recently developed membrane model, termed HMMM (Highly Mobile Membrane Mimetic) [59], an alternative membrane representation where lipid lateral diffusion is enhanced through the replacement of a large fraction of the phospholipid tail with an organic solvent yet still faithfully reproduces the energetics of membrane–protein interactions [59,60]. The enhanced lateral diffusion accelerates binding of αS by increasing the fluidity of the membrane; membrane headgroups can easily move to accommodate the incoming αS, as demonstrated by the accelerated binding of free lipid to HMMM bilayers [61]. Once bound, the increased fluidity of the membrane also lowers the barrier to further protein conformational changes within the membrane. Through repeated insertion of a helically folded αS, which is believed to best represent the fold of the protein in its membrane-bound form, into this dynamic membrane that maintains atomic detail, we arrive at an unbiased pool of 20 membrane associated states of αS.

These simulations have yielded new insight into the insertion process, as well as the conformational range αS adopts when bound to the membrane. In particular, we believe that we have isolated the initial stage of the postulated transition between membrane bound the broken-helix and extended-helix conformations, and can describe in detail the interactions that govern the transition.

Selected simulations were carried forward after the HMMM tails were extended through regrowing the shortened lipids towards their native length. The lipid tail regrowth algorithm leverages the atomic positions within the organic solvent to determine the locations of new carbon atoms added to the end of the tail. The resulting structure has longer tails, and as the structure is only mildly perturbed from a previous equilibrium run, is nearer to equilibrium than a newly regenerated membrane would be. Our results with the regrown membrane show agreement between short and longer lipids, indicating that the HMMM representation describes the binding mechanics while still permitting the membrane to sample space more rapidly.

## 2. Methods

The simulations performed were designed with the goal of arriving at an unbiased population of αS monomers inserted into the membrane. The approach was to begin with 20 copies of a helical model of αS as determined by NMR for a micelle-bound form of αS [33], place it above the membrane, and use the accelerated sampling and insertion of the HMMM [61] to arrive at a pool of membrane associated states of αS unbiased by its starting position along the membrane normal. In other words, we primarily aim at characterizing the depth of insertion and orientation of an already folded αS in the membrane, and not on describing the process of folding of the protein which is obviously beyond the timescales of atomistic simulations. This ensemble provides unparalleled statistics on the membrane-bound state of αS at an atomistic level. The details of system preparation and simulations are provided here.

### 2.1. System setup and simulation

A solution NMR αS structure (PDB ID: 2KKW [33]) was truncated beyond residue 100 as in earlier studies [52,54], and was placed 5 Å above 20 independently generated 120 × 120 Å$^2$ HMMM membranes [59]. Residue 100 is the approximate boundary between the N-terminal fragment known to adopt a predominantly α-helical membrane-bound structure and the free floating C-terminus [62]. The lipid composition of the membrane consisted of a 1:1 mixture of divalerylphosphatidylserine (DVPS) and divalerylphosphatidylcholine (DVPC) with an area per lipid of 75 Å$^2$/lipid (96 DVPS and 96 DVPC molecules per leaflet), a ratio chosen as a compromise between αS affinity to anionic phospholipids [22] and natural mammalian membrane compositions. The interior of the HMMM membrane was filled with 1,1-dichloroethane (DCLE) [59]. The area per lipid was chosen to be approximately 10% higher than what is expected for a native membrane [63], in order to allow for the asymmetric insertion of the αS monomer into one leaflet under the fixed-area ensemble required to maintain a physiological headgroup density. The measured area per lipid in the cis leaflet at the end of the simulations after the protein has inserted is 66.7 ± 0.5 Å$^2$/lipid, in line with lipid density of a relaxed membrane. Sodium and chloride ions were added using the *AUTOIONIZE* plugin of VMD [64] to neutralize each system and bring the salt concentration to 100 mM. A representative initial simulation system is shown in Fig. 1.

For each replicate, the following simulation protocol was used: with the protein held fixed, the membrane was equilibrated for 10 ns prior to an equilibrium NP$_n$AT simulation of 51 ns. Each replicate was simulated using NAMD 2.8 [65], CHARMM27 protein force field [66] and the CHARMM36 lipid force field [67], with a 2 fs time step. Non-bonded forces were calculated with a 12 Å cutoff (10 Å switching distance). Long-range electrostatic forces were calculated every other time step using the particle mesh Ewald method [68,69]. A Langevin thermostat using $\gamma = 1$ ps$^{-1}$ maintained the system temperature at 310 K. Pressure was maintained at 1 atm along the membrane normal using a Nosé–Hoover piston [70,71] with period and decay of 200 fs.

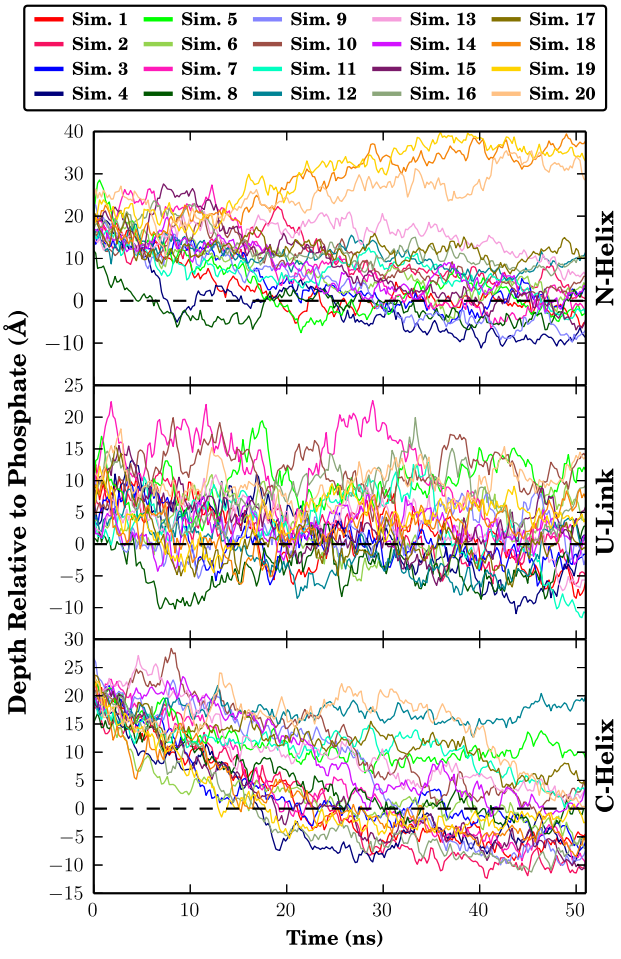


**Fig. 3.** Membrane insertion depth of αS. The height of the center of mass relative to the phosphate plane was calculated for the three sections of αS, namely the N-helix, U-link, and C-helix. Each simulation is represented by the same color in all panels. Over the last 5 ns, representing membrane-bound forms of αS in all simulations, the average insertion depth for the N-helix (residues 1–33) was $\mu_N = -0.7 \pm 5.7$ Å for all simulations except Simulations 12 and 18–20 where the N-helix did not fully insert. Likewise, the insertion depth for the C-helix (residues 45–92) was $\mu_C = 2.3 \pm 5.9$ Å for inserted C-termini. Insertion times are tabulated in Table S1.

### 2.2. Tail extension

While the HMMM efficiently and rapidly samples the membrane binding and insertion of the protein, a frequent concern is how the short acyl tails of HMMM bilayers impact equilibrium properties. In order to ensure that the final result has not been severely affected by the model's choice of acyl tail length, we extended the acyl tails by four carbons and monitored equilibrium properties. To extend the tails, we developed a method to grow the short lipid tails of the HMMM representation in a stepwise manner taking advantage of the atomic coordinates of the carbon atoms of the organic solvent as a guide. The extension protocol reverses the process of creating an HMMM membrane in a stepwise fashion by connecting the end of the lipid tails to the nearest solvent molecule. By using existing solvent atoms as the basis for the lengthened lipid tails, we try to minimize the perturbation of the membrane core, allowing for a faster relaxation of the system. Fig. 2 shows the steps within a single extension cycle schematically, summarizing the process of finding the nearest solvent molecule to a tail, applying patches to the structure, and reminimization of the structure to eliminate long bonds. Three systems were chosen from the pool of membrane-associated αS conformations and subjected to two rounds of tail extension, bringing the length of each lipidtail from 5 carbons to 9 carbons each. These systems with extended tails were simulated for an additional 15 ns using the same simulation protocol as described above.

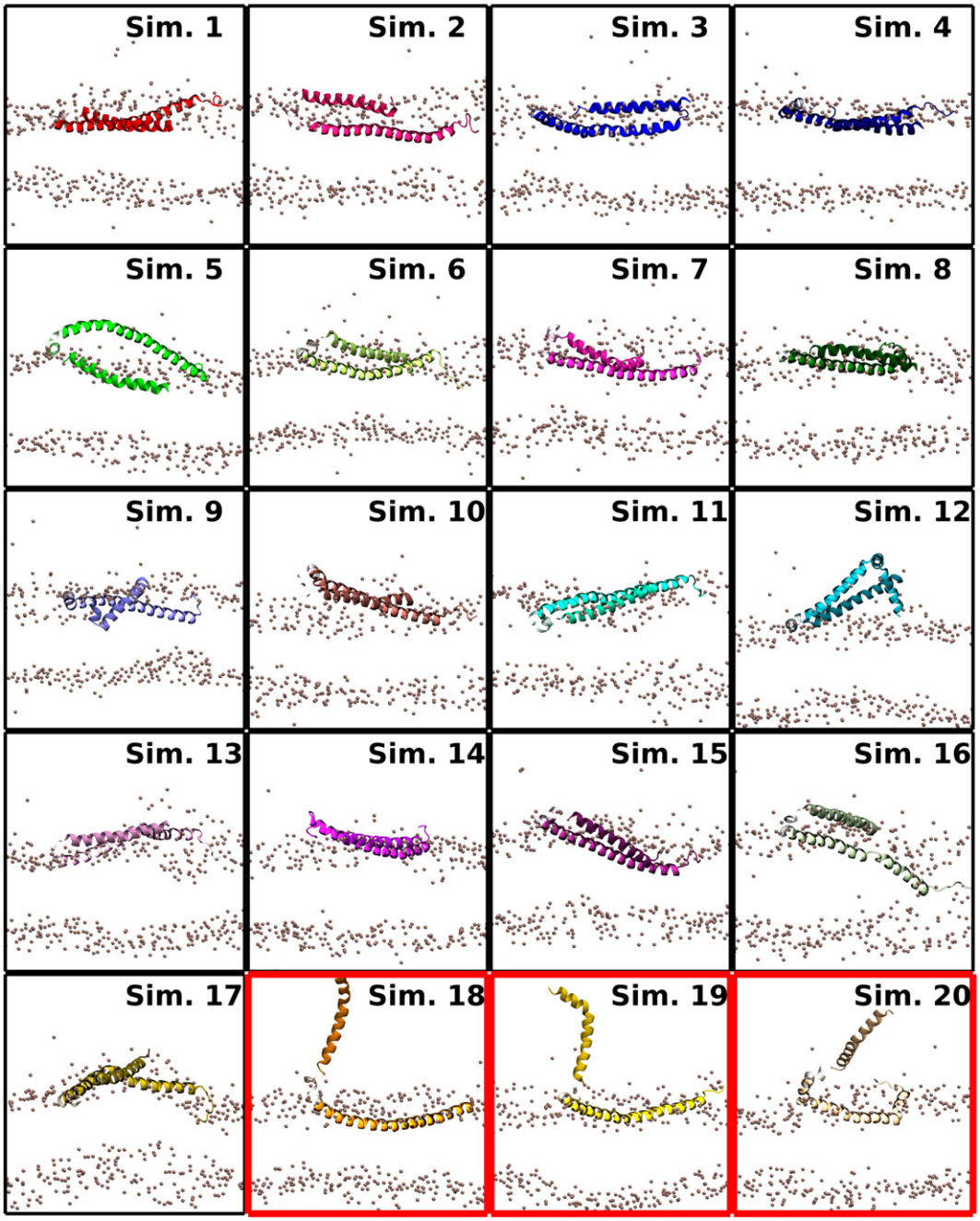


**Fig. 4.** Final membrane-bound αS states. A side view of the final state of the N- and C-helices from each simulation is shown. The position of phosphorus atoms in the two leaflets are given as bronze spheres. The N-helix is darker and shorter than the C-helix. The U-link between the helices is drawn using a transparent representation. Red borders around a state indicate simulations where the N-helix interacted across the periodic boundary.

### 2.3. Analysis

Purpose-built analysis VMD [64] scripts were devised to monitor quantities of interest, and eventual output plots generated by Matplotlib [72]. The depth of insertion was tracked for three regions of the protein. Residues 1–33, corresponding to the N-terminal α-helical segment, will be called the *N-helix*. Residues 45–92, corresponding to the C-terminal α-helical segment, will be called the *C-helix*. The region linking the two helices, corresponding to the tip of the U-shaped structure seen in NMR structures [33–35], will be called the *U-link* (residues 34–44). Residues 92–100 are ignored when monitoring the depth of insertion, as they are unstructured, and were initially included in the simulation to account for the long solvent-exposed tail. The membrane insertion depth was determined by the center of mass for all alpha carbons in a segment relative to the center of mass for all phosphorus atoms in the cis leaflet of the bilayer.

Local deviations from a straight α-helical structure are measured by the local kink angle ($\theta_k$), which measures the local helix kinking around residue $i$ by calculating the angle between the α carbons of the $i-4$th, $i$th, and $i+4$th residue. The relative orientation of the N-helix and C-helix is measured by the inter-helix angle ($\theta_h$), which measures the angle between least-squares linear fits of the N-helix and C-helix alpha carbons.

Specific sites of interaction between αS and the surrounding phospholipids were quantified by calculating a contact number over the last 15 ns of the trajectory, which represents the fully associated form in our simulations. The contact number for heavy atom $i$ of αS is given by:

$$C_i = \sum_{j \in lha} 1 - \frac{1}{1 + \exp\left(5\ \text{Å}^{-1}\left(d_{ij} - 4\ \text{Å}\right)\right)}$$

where *lha* is the set of lipid heavy atoms within 5 Å of atom $i$ and $d_{ij}$ is the distance between atoms $i$ and $j$. This formulation for contacts was originally designed for folding simulations [73], however we use it here to reweight contacts based on their distance, which is a proxy for strength.

To aid in the understanding of the results, the 20 independent simulations have been reindexed according to structural features that arose over the trajectories.

## 3. Results and discussion

### 3.1. Spontaneous membrane binding and insertion of αS

In each of the 20 independent simulations, the helical αS monomer is rapidly inserted into the membrane from its initial position 5 Å above the membrane. The insertion pattern of αS was not uniform, and different regions of αS are inserted into the membrane at different times, with complete membrane association and insertion occurring within 30 ns. On this short timescale, αS remains helical as it was in the starting micelle-bound NMR structure. The membrane insertion depth of each region was tracked by following the position of the alpha carbons along the membrane normal for each region (Fig. 3). Membrane insertions of the N-helix and C-helix are independent events, each typically embedding itself below the level of the phosphorus atoms of the surrounding phospholipids, with the insertion of the N-helix usually preceding that of the C-helix by an average of 5.4 ns (Table S1). The N-helix has been previously identified as being the catalyst of membrane association, with implications that the first four [48] or twelve [49] residues of αS promote membrane association and subsequent insertion, which is supported by the observed order of insertion in our simulations.

The final average insertion depths ($\mu$), taken to be the average insertion depth relative to the average membrane phosphorus position, over the last 5 ns, were computed for each segment. The final average insertion depths relative to phosphorus atoms of the cis leaflet were $\mu_N = -0.7 \pm 5.7$ Å for the N-helix, $\mu_U = -0.8 \pm 6.0$ Å for the U-link, and $\mu_C = 2.3 \pm 5.9$ Å for the C-helix. The average values capture the trend seen in earlier studies where the C-helix inserts more deeply into the bilayer [39,52]. Through repeating the simulation 20 times, and especially since the αS monomer was initially placed above the membrane rather than embedded within it, a greater variability in insertion depths is observed in our simulations. The accelerated dynamics of the HMMM allow αS to sample more extensively in the limited simulation time allotted. This allows us to capture for the first time with atomic-scale resolution the broad range of membrane-associated conformations that αS can adopt in the membrane [10,44,62]. This range of structures is recapitulated in Fig. 4, where the final frame from the 20 simulations depict significant variability in the degree of insertion of the individual helices. Very little of the insertion depth variability is ascribable to the organic solvent, as it is largely confined within 10 Å of the membrane center, which is well below the insertion depth of the average αS monomer.

As an additional check to extract out the effect of the organic solvent on the insertion depth, we can compare what happens when the simulations are extended after the short phospholipid tails are extended by four additional carbons. The depth of membrane insertion, reported in Fig. 5, shows the overall insertion depth relative to the surrounding membrane not to be affected by the extension of the lipid tails. Thus the wide distribution of equilibrium insertion depths does not appear

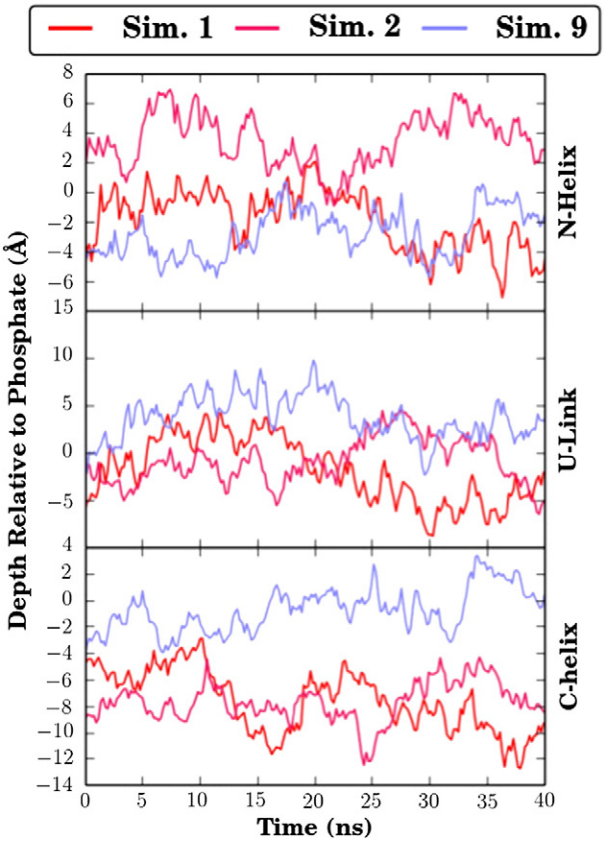


**Fig. 5.** Equilibrium insertion depth after lipid extension. As in Fig. 3, the height of the center of mass for three sections of αS was calculated for the three systems where the tails were extended. Line colors are consistent with Fig. 3. The membrane insertion depth is consistent with non-extended HMMM membranes, however the fluctuation of the penetration depth for a given trajectory is reduced. Over the last 15 ns of trajectory for a 5-carbon HMMM bilayer, the standard deviation of the insertion depth is 1.8 Å for a single trajectory. Once the HMMM bilayer is extended to 9-carbons, the deviation in insertion depth is only 1.3 Å over 15 ns. This indicates overall reduction in membrane flexibility with increasing acyl tail length.

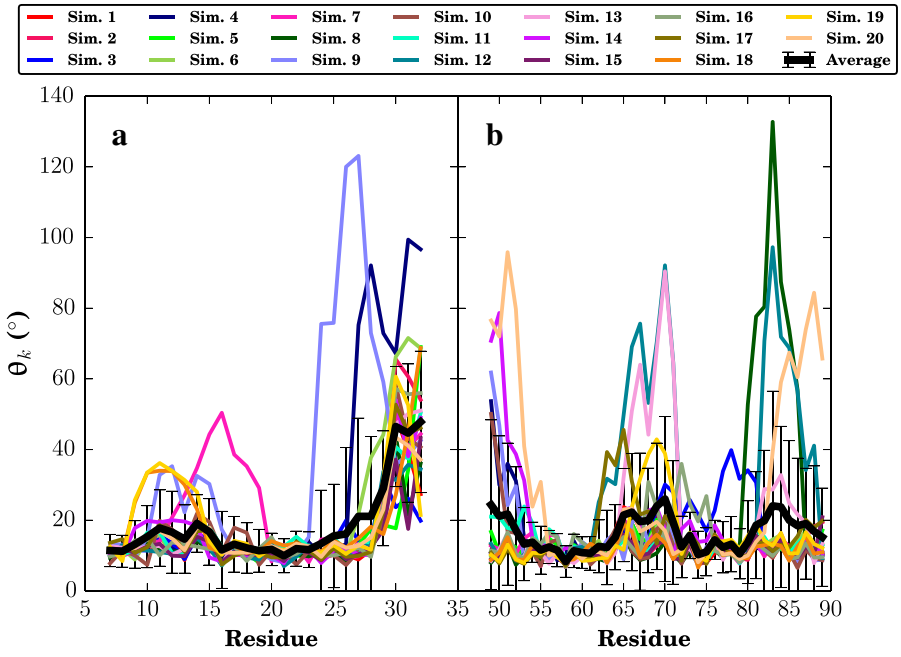


**Fig. 6.** Local kink angle ($\theta_k$). The local kink angle is defined as the average of the angle formed by the intersection of the vectors connecting the $\alpha$ carbon of residues $i-4$, $i$, and $i+4$ over the last 15 ns of simulation. The results for each simulation are given their own color, and the average and standard deviation of the local helix angle per residue shown with a thick black line. Panel (a) focuses on the N-helix region and likewise (b) focuses on the C-helix.

to be an artifact of using an HMMM representation, but rather a feature inherent to how $\alpha$S interacts with biological membranes.

The deviation in insertion depth within individual trajectories does decrease when the acylchains are extended. The reduced variability of the insertion depth after lipid extension is indicative of the extent to which acyl-chain length impacts membrane dynamics. The longer lipid tails do not simply retard the motions of the embedded protein laterally, but also present barriers to motion along the membrane normal. Using the standard deviation of insertion depth as a metric, we estimate that a protein in a membrane with acyl chains nine carbons long needs to be simulated twice as long to sample the same space as a protein in a membrane with acyl chains five carbons long. Assuming a linear dependence on chain length, simulations of peripheral proteins in conventional bilayers will need to be run at least 6–8 times longer to sample the same range of insertion depths as an HMMM membrane, an estimate that is congruent with the acceleration observed in membrane insertion [61].

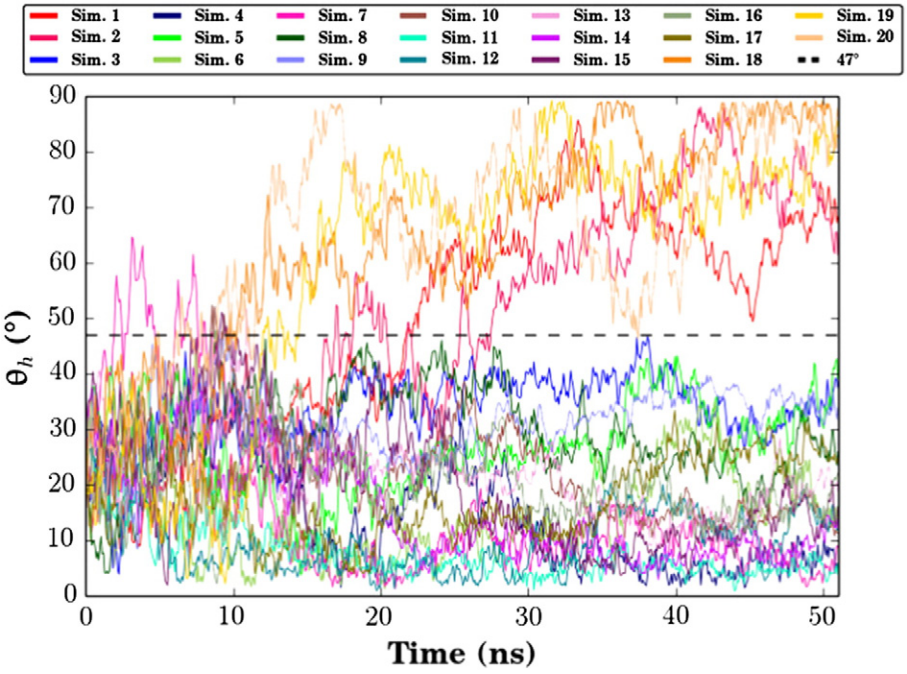


**Fig. 7.** Inter-helix angle ($\theta_h$). $\theta_h$ is defined by the angle between the two vectors formed by a linear interpolation of the $\alpha$ carbons of the N- and C-helices. The time series for each independent simulation are presented using a different color. Two distinguishable states emerge, a horseshoe-like state where $\theta_h$ never exceeds 47°, and a semi-extended state where the inter-helix angle approaches a right angle.

### 3.2. Bending of αS in its membrane-bound form

Prior atomistic simulations have quantified the degree of helical bending along the length of αS by measuring a local kink angle ($\theta_k$) as defined in the Methods [52]. This angle is designed to measure the local helical structure, values near 10° are expected for a prototypical α-helix; while larger values indicate a local helix-kink. Fig. 6 shows that in a typical trajectory, the N- and C-helices of αS are comparatively straight with only small kinks along the α-helices. In fact, αS only shows large kinks near the U-link region, residues 34–44 (Fig. S1). Qualitatively, the structures that emerge consistently are two stiff helical segments, linked together by the flexible U-link region where $\theta_k$ values are more varied and diverse. This qualitative description of αS helix dynamics within the HMMM membrane is consistent with prior experimental and computational studies, in which membrane-bound αS was predominantly helical [33–39,52].

Another important structural aspect of αS is the inter-helix angle ($\theta_h$) formed between the two comparatively stiff N- and C-helices. In the proposed extended conformation of αS, the angle formed by the junction of the N- and C-helices would be nearly 180°. Instead, NMR structures from micelles have shown the angle to be between 20 and 30°. Coarse-grained simulations and titration calorimetry have observed populations of both states [54,44], however atomistic simulations have not been able to capture this conformational diversity [52].

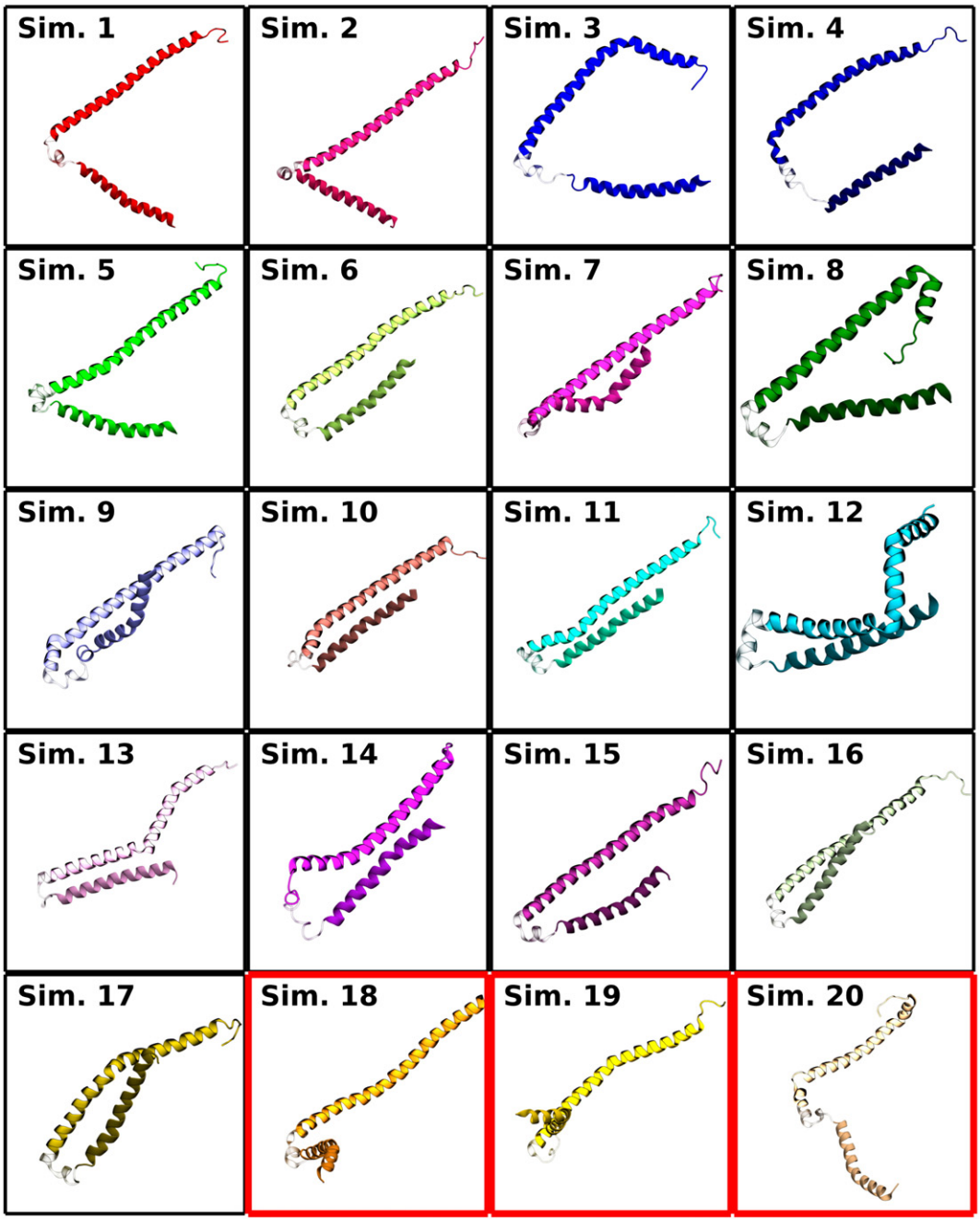


**Fig. 8.** Conformational heterogeneity of αS in membranes. The final conformations of αS from the 20 independent membrane binding simulations, as viewed from above the membrane. Each representation is colored consistently with Figs. 3 and 7, with the N-helix in the lower right quadrant and darker than the C-helix in the upper left quadrant the subplot, which results after aligning the structures in the membrane plane. Red borders around a state indicate simulations where the N-helix interacted across the periodic boundary. Secondary structure was assigned with STRIDE [75].

From our population pool of 20 membrane-bound αS simulations originating from the same NMR structure, we obtain a diverse set of inter-helix angles (Fig. 7). The final frames of the 20 simulations are presented graphically in Fig. 8. Broadly speaking, two populations are present in the simulations. The predominant population, comprising Simulations 3–17, is where $\theta_h$ never exceeds 47°, consistent with the initial NMR structure. In a minority of cases, comprising Simulations 1, 2, and 18–20, $\theta_h$ rises over the course of the simulation, approaching 90°. In the particular case of Simulations 18–20, $\theta_h$ increases due to the N-helix interacting with both leaflets across the periodic image while the C-helix interacts with a single leaflet. This is a simulation artifact that likely has a little meaning for αS function in vivo, aside from demonstrating the flexibility of the broken helix conformation of αS. For Simulations 1 and 2, the increase in $\theta_h$ occurs as the αS monomers are inserting into the membrane, suggesting that interactions with the membrane interface can drive changes in the structure of αS away from the initial broken-helix conformation taken from NMR structures, and towards the extended conformation seen on bilayers. While the $\theta_h$ does not cross the 47 degree threshold in Simulations 3 and 4, the N-helix and C-helix are well separated from one another in the end state, suggesting that these simulations may also be transitioning towards an extended-helix conformation.

Extending Simulations 1, 2 and 9, after membrane extension, confirms that $\theta_h$ was not impacted by acyl tail length. The $\theta_h$ values within the extended membrane simulations (Fig. S2) are approximately constant, varying within 10° of their initial values over the 15 ns of

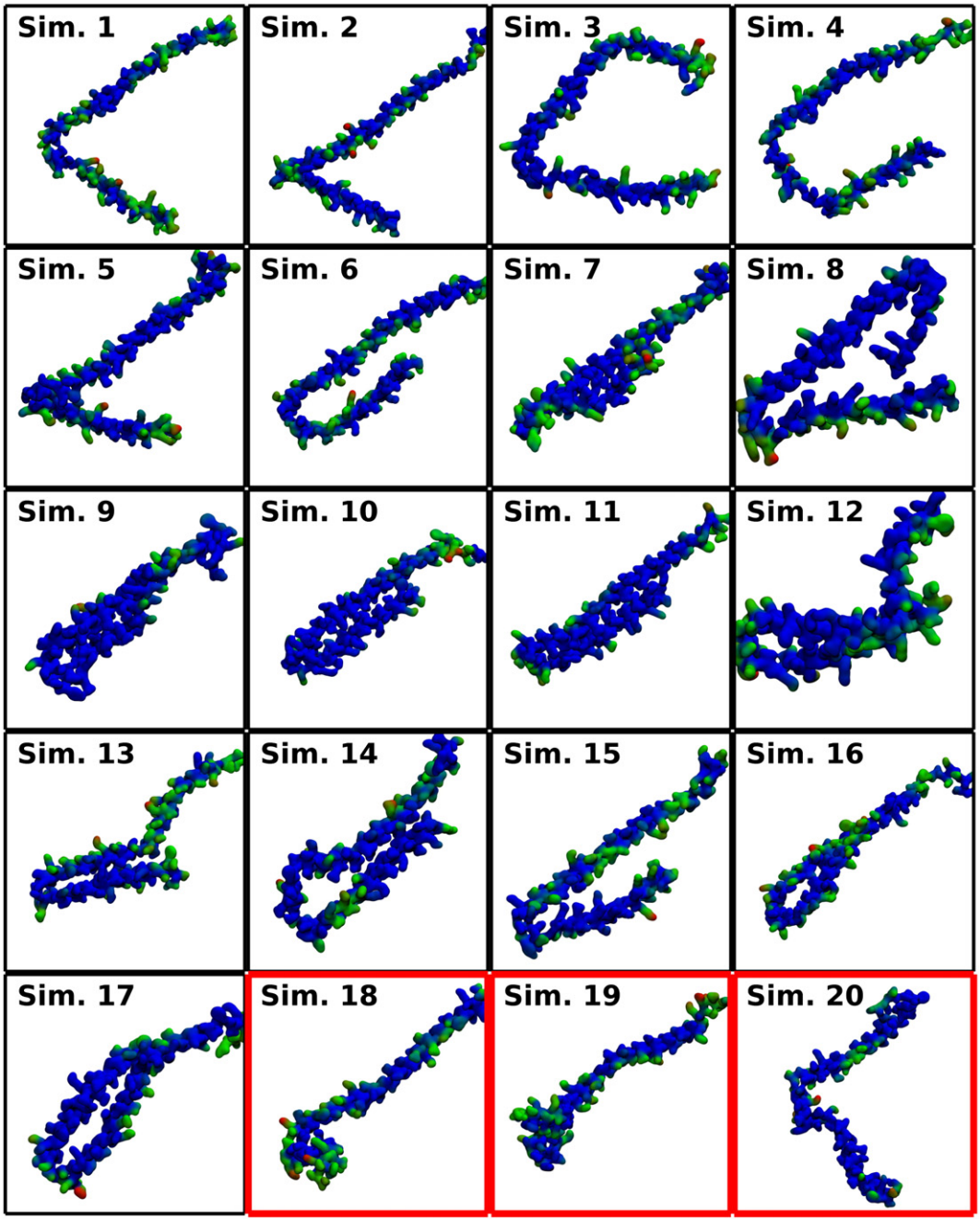


**Fig. 9.** PS-contact map. A top view of the protein in its final state (a view equivalent to Fig. 8) where each atom has been color coded according to the number of contacts with PS-headgroups over the last 15 ns of simulation (blue for no contacts, green for some, and red for many). The resulting Quicksurf [74] surface highlights specific interaction sites on the protein. PDB structures of final αS states are available as supplemental materials, with the number of PS contacts coded into the beta field.

extended simulations. The low variability of $\theta_h$ in the extended membrane suggests that the observed states where $\theta_h$ is larger, and the αS monomer is transitioning towards an extended state are stable within a bilayer composed of longer lipids, and given longer sampling times, might result in a fully extended structure. Our interpretation is that the HMMM representation of the membrane, with its inherently more fluid membrane, allowed us to escape the kinetic trap that confined previous atomistic simulations to sample only the broken-helix state.

### 3.3. Membrane interaction and linearization of αS

αS binds to negatively charged membranes, but not to neutral membrane components [22,25]. This implies the existence of specific interactions between αS side chains and negatively charged lipids in the membrane, interactions that may play a role in the linearization of αS. Taking advantage of the atomistic nature of the HMMM model we track the detailed interactions between the lipid headgroups and αS which might be responsible for the angular response of αS. Given the conformational flexibility of αS, observation of the same exact interactions over 20 independent trajectories is extremely unlikely, and so instead we are tasked to any pattern of interaction that might influence whether an individual trajectory will transition towards an extended conformation or remain in the original broken helix conformation observed in NMR experiments [33–35].

Using the metric of lipid contact number to highlight regions of αS that interact extensively with the PS and PC headgroups of the membrane, it is possible to elucidate some general trends (Fig. 9 for PS contacts and Fig. S3 PC contacts). In Simulations 1–4, where the N- and C-helices are well separated and represent a semi-extended helix, there are clear interactions along the interfacial edges between the N- and C-helices and PS headgroups. For Simulations 5–17, which represent a membrane-bound broken helix of αS, there are demonstrably fewer PS contacts along the inner face (Fig. 9). Tabulating the contact numbers by residue (Table S2 for PS, Table S3 for PC), an increase in the total number of contacts for Simulations 1–4 relative to Simulations 5–17 becomes evident, a result of the greater surface area exposed in the semi-extended conformation of αS. The increase is greater in the number of PS-Lys contacts formed in the semi-extended state (Sim. 1–4), suggesting that there is a possibility for salt-bridges to form between the N- and C-helices that would stabilize the broken-helix conformation found in the NMR structure. These interactions would need to be disrupted before linearization of the broken-helix conformation could take place.

Evidence of such interactions can be found in the broken helix trajectories from Simulations 5–17, where contacts are observed to form between the N- and C-helices.

The observed exact bonding patterns, as exemplified in Fig. 10, are not unique, and result in different topological constraints on the protein. Depending on small rotations along the helical axes, different hydrogen bonds between the N- and C-helices form. The hydrogen bonds are largely confined to the same range of residues, between charged residues in the 54–62 range and polar ones from residues 21–28. For a transition towards an extended conformation, these interactions must be replaced with equally favorable ones, such as the interactions to the surrounding lipids. The access of these alternative bonding partners to the protein promotes the transition between the broken-helix and extended helix membrane-bound αS conformations.

## 4. Conclusion

In this study, we employed atomistic MD simulations to arrive at an unbiased pool of αS monomers bound to lipid bilayers, and to investigate the dynamics of its membrane-bound form. By leveraging the accelerated sampling of an alternative membrane representation allowing for repeated (20) simulations, we not only capture the conformational heterogeneity of membrane-bound αS in independent simulations, but also collect sufficient data to report for the first time the influence of membrane interactions on the conformational states of αS at an atomistic level of detail. Furthermore, in a number of simulations, αS was found to undergo a transition from the initial broken-helix conformation, which was adopted from the starting NMR structure, to a semi-extended conformation. The observed transition, which is suggested to occur at equilibrium [42–44], implies that prior atomistic simulations may have underestimated the natural variability within the membrane-bound structure of αS. The transition between the broken- and extended-helix conformations would likely also occur in a conventional model bilayer, however the timescale needed would be much longer than those currently achievable by atomistic simulations. Indeed, inducing complete transition to a fully extended state in an atomic simulation to obtain a free energy profile requires sampling timescales that are currently inaccessible. Under equilibrium conditions, these transitions are stochastic events, and can only be captured with methods and models offering more robust sampling. Using our previous estimate of the increased sampling rate of a peripheral protein in an HMMM bilayer, the simulations here might be roughly equivalent to 6–8 μs of equilibrium simulation of an αS monomer in a conventional membrane with a comparable lipid composition. It has to be noted however that while the dynamics of the lipids have been enhanced with the application of the HMMM membrane, the conformational dynamics of the protein component, though less hampered by the slow lipid dynamics here, are still governed by molecular events that continue to be slow, such as protein folding, which are best sampled using coarse grained approaches [54]. Therefore, even with the HMMM membrane, we have not been able to capture the entire process of membrane-induced conformational changes in αS, though we have isolated specific interhelical hydrogen bonds that can stabilize the broken-helix conformation.

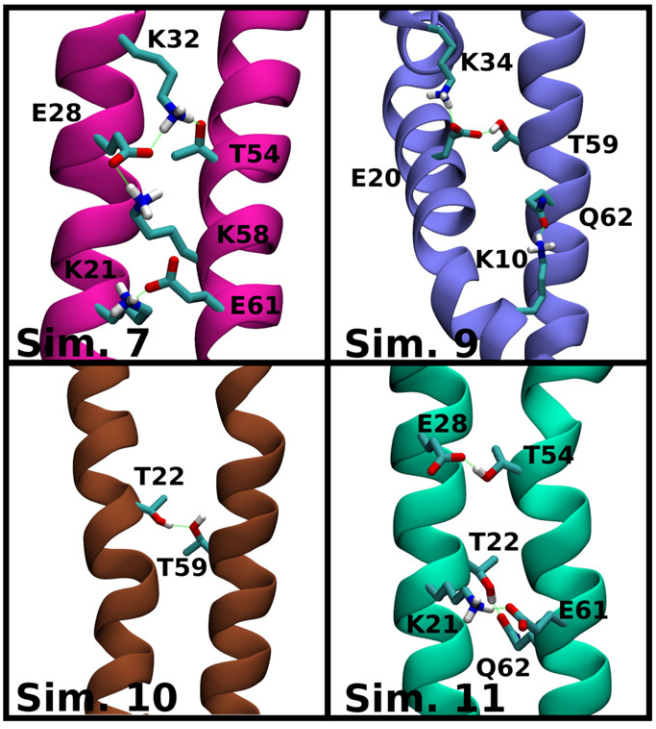


**Fig. 10.** Representative inter-helix hydrogen bonds stabilizing the horseshoe conformation. Snapshots are color-coded and labeled according to the simulation of origin. Prevalent hydrogen bonds between residues on the N- and C-helices are highlighted in green, and the interacting side chains are labeled and shown with the following color mapping: carbon atoms are cyan, oxygen atoms are red, nitrogen atoms are blue, and hydrogen atoms involved in hydrogen bonding are shown in white. All other atoms are omitted for clarity. Note that the K21–E61 interaction is the most prevalent, appearing in Simulations 7, 11, 13, and 15 (13 and 15 not shown).

## Acknowledgments

This research is supported by the National Institutes of Health grants R01-GM101048, R01-GM086749, U54-GM087519, and P41-GM104601. We gratefully acknowledge the past and present support of both the NIH Molecular Biophysics Training Grant, and a DOE Computational Sciences Graduate Fellowship, supported by grant DE-FG02-97ER25308. This work used the Extreme Science and Engineering Discovery Environment (XSEDE), which is supported by National Science Foundation grant number OCI-1053575. These particular computations were performed on Ranger and Stampede at the Texas Advanced Computing Center (TACC) within the University of Texas at Austin and on Kraken at the National Institute for Computational Sciences (http://www.nics.tennessee.edu/) (XSEDE grant number MCA06N060).

## Appendix A. Supplementary data

Supplementary data to this article can be found online at http://dx.doi.org/10.1016/j.bbamem.2014.08.012.

## References

[1] J. Burré, M. Sharma, T. Tsetsenis, V. Buchman, M.R. Etherton, T.C. Südhof, α-Synuclein promotes SNARE-complex assembly in vivo and in vitro, Science 329 (2010) 1663–1667.
[2] J. Diao, J. Burré, S. Vivona, D.J. Cipriano, M. Sharma, M. Kyoung, T.C. Südhof, A.T. Brunger, Native α-synuclein induces clustering of synaptic-vesicle mimics via binding to phospholipids and synaptobrevin-2/VAMP2, eLife 2 (2013) e00592.
[3] A.J. Lees, J. Hardy, T. Revesz, Parkinson's disease, Lancet 373 (2009) 13–19.
[4] M.G. Spillantini, M.L. Schmidt, V.M.-Y. Lee, J.Q. Trojanowski, R. Jakes, M. Goedert, α-Synuclein in Lewy bodies, Nature 388 (1997) 839–840.
[5] M.H. Polymeropoulous, C. Lavedan, E. Leroy, S.E. Ide, A. Deheija, A. Dutra, B. Pike, H. Root, J. Rubenstein, R. Boyer, E.S. Stenroos, S. Chandrasekharappa, A. Athanassiadou, T. Papapetropoulous, W.G. Johnson, A.M. Lazzarini, R.C. Duvosin, G.D. Iorio, L.I. Golbe, R.L. Nussbaum, Mutation in the α-synuclein gene identified in families with Parkinson's disease, Science 276 (1997) 2045–2047.
[6] R. Krüger, W. Kuhn, T. Müller, D. Woitalla, M. Graeber, S. Kösel, H. Przuntek, J.T. Epplen, L. Schols, O. Riess, AlaSOPro mutation in the gene encoding α-synuclein in Parkinson's disease, Nat. Genet. 18 (1998) 106–108.
[7] J.J. Zarranz, J. Alegre, J.C. Gomez-Esteban, E. Lezcano, R. Ros, I. Ampuero, L. Vidal, J. Hoenicka, O. Rodriguez, B. Atares, V. Llorens, E.G. Tortosa, T. del Ser, D.G. Munoz, J. G. de Yebenes, The new mutation, E46K, or alpha-synuclein causes Parkinson and Lewy Body dementia, Ann. Neurol. 55 (2004) 164–173.
[8] M.-C. Chartier-Harlin, J. Kachergus, C. Roumier, V. Mouroux, X. Douay, S. Lincoln, C. Levecque, L. Larvor, J. Andrieux, M. Hulihan, N. Waucquier, L. Defebvre, P. Amouyel, M. Farrer, A. Destée, α-Synuclein locus duplication as a cause of familial Parkinson's disease, Lancet 364 (2004) 1167–1169.
[9] A.B. Singleton, M. Farrer, J. Johnson, A. Singleton, S. Hague, J. Kachergus, M. Hulihan, T. Peuralinna, A. Dutra, R. Nussbaum, S. Lincoln, A. Crawley, M. Hanson, D. Maraganore, C. Adler, M.R. Cookson, M. Muenter, M. Baptista, D. Miller, J. Blancato, J. Hardy, K. Gwinn-Hardy, α-Synuclein locus triplication causes Parkinson's disease, Science 302 (2003) 841.
[10] I. Dikiy, D. Eliezer, Folding and misfolding of alpha-synuclein on membranes, Biochim. Biophys. Acta Biomembr. 1818 (2012) 1013–1018.
[11] D. Boassa, M.L. Berlanga, M.A. Yang, M. Terada, J. Hu, E.A. Bushong, M. Hwang, E. Masliah, J.M. George, M.H. Ellisman, Mapping the subcellular distribution of α-synuclein in neurons using genetically encoded probes for correlated light and electron microscopy: implications for Parkinson's disease pathogenesis, J. Neurosci. 33 (2013) 2605–2615.
[12] A. Iwai, E. Masliah, M. Yoshimoto, N. Ge, L. Flanagan, H.R. de Silva, A. Kittel, T. Saitoh, The precursor protein of non-Aβ component of Alzheimer's disease amyloid is a presynaptic protein of the central nervous system, Neuron 14 (1995) 467–475.
[13] D.F. Clayton, J.M. George, The synucleins: a family of proteins involved in synaptic function, plasticity, neurodegeneration and disease, Trends Neurosci. 21 (1998) 249–254.
[14] C.G. Dudzik, E.D. Walter, B.S. Abrams, M.S. Jurica, G.L. Millhauser, Coordination of copper to the membrane-bound form of α-synuclein, Biochemistry 52 (2013) 53–60.
[15] D.D. Murphy, S.M. Rueter, J.Q. Trojanowski, V.M. Lee, Synucleins are developmentally expressed, and α-Synuclin regulates the size of the presynaptic vesicular pool in primary hippocampal neurons, J. Neurosci. 20 (2000) 3214–3220.
[16] D.E. Cabin, K. Shimazu, D. Murphy, N.B. Cole, W. Gottschalk, K.L. Mcllwain, B. Orrison, A. Chen, C.E. Ellis, R. Paylor, B. Lu, R.L. Nussbaum, Synaptic vesicle depletion correlates with attenuated synaptic responses to prolonged repetitive stimulation in mice lacking α-synuclein, J. Neurosci. 15 (2002) 8787–8807.
[17] L. Yavich, H. Tanila, S. Vepsäläinen, P. Jäkälä, Role of α-synuclein in presynaptic dopamine recruitment, J. Neurosci. 8 (2004) 11165–11170.
[18] S. Liu, I. Ninan, I. Antonova, F. Battaglia, F. Trinchese, A. Narasanna, N. Kolodilov, W. Dauer, R.D. Hawkins, O. Arancio, α-Synuclein produces a long-lasting increase in neurotransmitter release, EMBO J. 23 (2004) 4506–4516.
[19] G. Rodriguez-Araujo, H. Nakagami, H. Hayashi, M. Mori, T. Shiuchi, Y. Minokoshi, Y. Nakaoka, Y. Takami, I. Komuro, R. Morishita, Y. Kaneda, Alpha-synuclein elicits glucose uptake and utilization in adipocytes through the Gab1/PI3K/Akt transduction pathway, Cell. Mol. Life Sci. 70 (2013) 1123–1133.
[20] T.L. Yap, J.M. Gruschus, A. Velyati, W. Westbroek, E. Goldin, N. Moaven, E. Sidransky, J.C. Lee, α-Synuclein interacts with glucocerebrosidase providing a molecular link between Parkinson and Gaucher diseases, J. Biol. Chem. 286 (2011) 28080–28088.
[21] B.-H. Ahn, H. Rhim, S.Y. Kim, Y.-M. Sung, M.-Y. Lee, J.-Y. Choi, B. Wolozin, J.-S. Chang, Y.H. Lee, T.K. Kwon, S.-H. Yoon, S.J. Hahn, M.-S. Kim, Y.-H. Jo, D.S. Min, α-Synuclein interacts with phospholipase D isozymes and inhibits pervanadate-induced phospholipase D activation in human embryonic kidney-293 cells, J. Biol. Chem. 277 (2002) 12334–12342.
[22] E. Jo, J. McLaurin, C.M. Yip, P.S. George-Hyslop, P.E. Fraser, α-Synuclein membrane interactions and lipid specificity, J. Biol. Chem. 275 (2000) 34328–34334.
[23] A.P. Pandey, F. Haque, J.-C. Rochet, J.S. Hovis, Clustering of α-synuclein on supported lipid bilayers: role of anionic lipid, protein, and divalent ion concentration, Biophys. J. 96 (2009) 540–551.
[24] M. Necula, C.N. Chirita, J. Kuret, Rapid anionic micelle-mediated α-synuclein fibrillization in vitro, J. Biol. Chem. 278 (2003) 46674–46680.
[25] E. Hellstrand, M. Grey, M.-L. Ainalem, J. Ankner, V.T. Forsyth, G. Fragneto, M. Haertlein, M.-T. Dauvergne, H. Nilsson, P. Brundin, S. Linse, T. Nylander, E. Sparr, Adsorption of α-synuclein to supported lipid bilayers: positioning and role of electrostatics, ACS Chem. Neurosci. 4 (2013) 1339–1351.
[26] M. Grey, S. Linse, H. Nilsson, P. Brundin, E. Sparr, Membrane interaction of α-synuclin in different aggregation states, J. Park. Dis. 1 (2011) 359–371.
[27] L. Tosatto, A.O. Andrighetti, N. Plotegher, V. Antonini, I. Tessari, L. Ricci, L. Bubacco, M. Dalla Serra, Alpha-synuclein pore forming activity upon membrane association, Biochim. Biophys. Acta Biomembr. 1818 (2012) 2876–2883.
[28] I.F. Tsigelny, Y. Sharikov, W. Wrasidlo, T. Gonzalez, P.A. Desplats, L. Crews, B. Spencer, E. Masliah, Role of α-synuclein penetration into the membrane in the mechanisms of oligomer pore formation, FEBS J. 279 (2012) 1000–1013.
[29] B. Winner, R. Jappelli, S.K. Maji, P.A. Desplats, L. Boyer, S. Aigner, C. Hetzer, T. Loher, M. Vilar, S. Campioni, C. Tzitzilonis, A. Soragni, S. Jessberger, H. Mira, A. Consiglio, E. Pham, E. Masliah, F.H. Gage, R. Riek, In vivo demonstration that α-synuclein oligomers are toxic, Proc. Natl. Acad. Sci. U. S. A. 108 (2011) 4194–4199.
[30] M.J. Volles, S.-J. Lee, J.-C. Rochet, M.D. Shtilerman, T.T. Ding, J.C. Kessler, P.T. Lansbury Jr., Vesicle permeabilization by protofibrillar α-synuclein: implications for the pathogenesis and treatment of Parkinson's disease, Biochemistry 40 (2001) 7812–7819.
[31] J. Wietek, I. Haralampiev, A. Amoussouvi, A. Herrmann, M. Stöckl, Membrane bound α-synuclein is fully embedded in the lipid bilayer while segments with higher flexibility remain, FEBS Lett. 587 (2013) 2572–2577.
[32] T. Bartels, J.G. Choi, D.J. Selkoe, α-Synuclein occurs physiologically as a helically folded tetramer that resists aggregation, Nature 477 (2011) 107–110.
[33] J.N. Rao, C.C. Jao, B.G. Hegde, R. Langen, T.S. Ulmer, A combinatorial NMR and EPR approach for evaluating the structural ensemble of partially folded proteins, J. Am. Chem. Soc. 132 (2010) 8657–8668.
[34] M. Drescher, G. Veldhuis, B.D. van Rooijen, S. Milikisyants, V. Subramaniam, M. Huber, Antiparallel arrangement of the helices of vesicle-bound α-synuclein, J. Am. Chem. Soc. 130 (2008) 7796–7797.
[35] T.S. Ulmer, A. Bax, N.B. Cole, R.L. Nussbaum, Structure and dynamics of micelle-bound human alpha-synuclein, J. Biol. Chem. 280 (2005) 9595–9603.
[36] A.J. Trexler, E. Rhoades, α-Synuclein binds large unilamellar vesicles as an extended helix, Biochemistry 48 (2009) 2304–2306.
[37] E.R. Georgieva, T.F. Ramlall, P.P. Borbat, J.H. Freed, D. Eliezer, Membrane-bound alpha-synuclein forms an extended helix: long-distance pulsed ESR measurements using vesicles, bicelles and rod-like micelles, J. Am. Chem. Soc. 130 (2008) 12856–12857.
[38] C.C. Jao, B.G. Hegde, J. Chen, I.S. Haworth, R. Langen, Structure of membrane-bound α-synuclein from site-directed spin labeling and computational refinement, Proc. Natl. Acad. Sci. U. S. A. 105 (2008) 19666–19671.
[39] C.C. Jao, A. Der-Sarkissian, J. Chen, R. Langen, Structure of membrane-bound α-synuclein studied by site-directed spin-labeling, Proc. Natl. Acad. Sci. U. S. A. 101 (2004) 8331–8336.
[40] P. Borbat, T.F. Ramlall, J.H. Freed, D. Eliezer, Inter-helix distances in lysophospholipid micelle-bound α-synuclein from pulsed ESR measurements, J. Am. Chem. Soc. 128 (2006) 10004–10005.
[41] E.R. Middleton, E. Rhoades, Effects of curvature and composition on α-synuclein binding to lipid vesicles, Biophys. J. 99 (2010) 2279–2288.
[42] M. Robotta, P. Braun, B. van Rooijen, V. Subramaniam, M. Huber, M. Drescher, Direct evidence of coexisting horseshoe and extended helix conformations of membrane-bound alpha-synuclein, ChemPhysChem 12 (2011) 267–269.
[43] E.R. Georgieva, T.F. Ramlall, P.P. Borbat, J.H. Freed, D. Eliezer, The lipid-binding domain of wild type and mutant α-synuclein: compactness and interconversion between the broken and extended helix forms, J. Biol. Chem. 285 (2010) 28261–28274.
[44] S.B. Lokappa, T.S. Ulmer, Alpha-synuclein populates both elongated and broken helix states on small unilamellar vesicles, J. Biol. Chem. 286 (2011) 21450–21457.
[45] G. Comellas, L.R. Lemkau, D.H. Zhou, J.M. George, C.M. Rienstra, Structural intermediates during α-synuclein fibrillogenesis on phospholipid vesicles, J. Am. Chem. Soc. 134 (2012) 5090–5099.
[46] K. Vamvaca, M.J. Volles, P.T. Lansbury Jr., The first N-terminal amino acids of α-synuclein are essential for α-helical structure formation in vitro and membrane binding in yeast, J. Mol. Biol. 389 (2009) 413–424.

[47] T. Bartels, L.S. Ahlstrom, A. Leftin, F. Kamp, C. Haass, M.F. Brown, K. Beyer, The N-terminus of the intrinsically disordered protein α-synuclein triggers membrane binding and helix folding, Biophys. J. 99 (2010) 2116–2124.
[48] C.M. Pfefferkorn, F. Heinrich, A.J. Sodt, A.S. Maltsev, R.W. Pastor, J.C. Lee, Depth of α-synuclein in a bilayer determined by fluorescence, neutron reflectometry, and computation, Biophys. J. 102 (2012) 613–621.
[49] A.S. Maltsev, J. Ying, A. Bax, Impact of N-terminal acetylation of α-synuclein on its random coil and lipid binding properties, Biochemistry 51 (2012) 5004–5013.
[50] I. Dikiy, D. Eliezer, N-terminal acetylation stabilizes N-terminal helicity in lipid- and micelle-bound alpha-synuclein and increases its affinity for physiological membranes, J. Biol. Chem. 289 (2014) 3652–3665.
[51] N. Lorenzen, L. Lemminger, J.N. Pedersen, S.r.B. Nielsen, D.E. Otzen, The N-terminus of α-synuclein is essential for both monomeric and oligomeric interactions with membranes, FEBS Lett. 588 (2014) 497–502.
[52] J.D. Perlmutter, A.R. Braun, J.N. Sachs, Curvature dynamics of α-synuclein familial Parkinson disease mutants, J. Biol. Chem. 284 (2009) 7177–7189.
[53] I.F. Tsigelny, P. Bar-On, Y. Sharikov, L. Crews, M. Hashimoto, M.A. Miller, S.H. Keller, O. Platoshyn, J.X.-J. Yuan, E. Masliah, Dynamics of α-synuclein aggregation and inhibition of pore-like oligomer development by β-synuclein, FEBS J. 274 (2007) 1862–1877.
[54] A.R. Braun, E. Sevcsik, P. Chin, E. Rhoades, S. Tristram-Nagle, J.N. Sachs, α-Synuclein induces both positive mean curvature and negative Gaussian curvature in membranes, J. Am. Chem. Soc. 134 (2012) 2613–2620.
[55] J.B. Klauda, B.R. Brooks, R.W. Pastor, Dynamical motions of lipids and a finite size effect in simulations of bilayers, J. Chem. Phys. 125 (2006) 144710.
[56] J. Wohlert, O. Edholm, Dynamics in atomistic simulations of phospholipid membranes: nuclear magnetic resonance relaxation rates and lateral diffusion, J. Chem. Phys. 125 (2006) 204703.
[57] S.J. Marrink, H.J. Risselada, S. Yefimov, D.P. Tieleman, A.H. de Vries, The MARTINI force field: coarse grained model for biomolecular simulations, J. Phys. Chem. B 111 (2007) 7812–7824.
[58] P.S. Coppock, J.T. Kindt, Atomistic simulations of mixed-lipid bilayers in gel and fluid phases, Langmuir 25 (2009) 352–359.
[59] Y.Z. Ohkubo, T.V. Pogorelov, M.J. Arcario, G.A. Christensen, E. Tajkhorshid, Accelerating membrane insertion of peripheral proteins with a novel membrane mimetic model, Biophys. J. 102 (2012) 2130–2139.
[60] T.V. Pogorelov, J.V. Vermaas, M.J. Arcario, E. Tajkhorshid, Partitioning of amino acids into a model membrane: capturing the interface, J. Phys. Chem. B 118 (2014) 1481–1492.
[61] J.V. Vermaas, E. Tajkhorshid, A microscopic view of phospholipid insertion into biological membranes, J. Phys. Chem. B 118 (2014) 1754–1764.
[62] D. Eliezer, E. Kutluay, R. Bussell, G. Browne, Conformational properties of alpha-synuclein in its free and lipid-associated states, J. Mol. Biol. 307 (2001) 1061–1073.
[63] J.F. Nagle, S. Tristram-Nagle, Structure of lipid bilayers, Biochim. Biophys. Acta 1469 (2000) 159–195.
[64] W. Humphrey, A. Dalke, K. Schulten, VMD — visual molecular dynamics, J. Mol. Graphics 14 (1996) 33–38.
[65] J.C. Phillips, R. Braun, W. Wang, J. Gumbart, E. Tajkhorshid, E. Villa, C. Chipot, R.D. Skeel, L. Kale, K. Schulten, Scalable molecular dynamics with NAMD, J. Comput. Chem. 26 (2005) 1781–1802.
[66] A.D. MacKerell Jr., M. Feig, C.L. Brooks III, Extending the treatment of backbone energetics in protein force fields: limitations of gas-phase quantum mechanics in reproducing protein conformational distributions in molecular dynamics simulations, J. Comput. Chem. 25 (2004) 1400–1415.
[67] J.B. Klauda, R.M. Venable, J.A. Freites, J.W. O'Connor, D.J. Tobias, C. Mondragon-Ramirez, I. Vorobyov, A.D. MacKerell Jr., R.W. Pastor, Update of the CHARMM all-atom additive force field for lipids: validation on six lipid types, J. Phys. Chem. B 114 (2010) 7830–7843.
[68] T. Darden, D. York, L.G. Pedersen, Particle mesh Ewald: an $N\cdot\log(N)$ method for Ewald sums in large systems, J. Chem. Phys. 98 (1993) 10089–10092.
[69] U. Essmann, L. Perera, M.L. Berkowitz, T. Darden, H. Lee, L.G. Pedersen, A smooth particle mesh Ewald method, J. Chem. Phys. 103 (1995) 8577–8593.
[70] G.J. Martyna, D.J. Tobias, M.L. Klein, Constant pressure molecular dynamics algorithms, J. Chem. Phys. 101 (1994) 4177–4189.
[71] S.E. Feller, Y. Zhang, R.W. Pastor, B.R. Brooks, Constant pressure molecular dynamics simulation: the Langevin piston method, J. Chem. Phys. 103 (1995) 4613–4621.
[72] J.D. Hunter, Matplotlib: a 2D graphics environment, Comput. Sci. Eng. 9 (2007) 90–95.
[73] F.B. Sheinerman, C.L. Brooks III, Calculations on folding of segment B1 of streptococcal protein G, J. Mol. Biol. 278 (1998) 439–456.
[74] M. Krone, J.E. Stone, T. Ertl, K. Schulten, Fast visualization of Gaussian density surfaces for molecular dynamics and particle system trajectories, EuroVis — Short Papers 2012, 2012, pp. 67–71.
[75] D. Frishman, P. Argos, Knowledge-based secondary structure assignment, Proteins 23 (1995) 566–579.